

A Crossed Molecular Beam and Ab-Initio Investigation of the Reaction of Boron Monoxide (BO; $X^2\Sigma^+$) with Methylacetylene (CH_3CCH ; X^1A_1): Competing Atomic Hydrogen and Methyl Loss Pathways

Surajit Maity, Dorian S. N. Parker, Beni B. Dangi, and Ralf I. Kaiser*

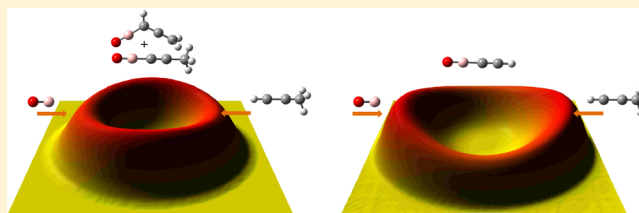
Department of Chemistry, University of Hawai'i at Manoa, Honolulu, Hawaii 96822, United States

Stefan Fau, Ajith Perera, and Rodney J. Bartlett*

Quantum Theory Project, University of Florida, Gainesville, Florida 32611, United States

Supporting Information

ABSTRACT: The gas-phase reaction of boron monoxide (^{11}BO ; $X^2\Sigma^+$) with methylacetylene (CH_3CCH ; X^1A_1) was investigated experimentally using crossed molecular beam technique at a collision energy of 22.7 kJ mol^{-1} and theoretically using state of the art electronic structure calculation, for the first time. The scattering dynamics were found to be indirect (complex forming reaction) and the reaction proceeded through the barrier-less formation of a van-der-Waals complex ($^{11}\text{BOC}_3\text{H}_4$) followed by isomerization via the addition of $^{11}\text{BO}(X^2\Sigma^+)$ to the C1 and/or C2 carbon atom of methylacetylene through submerged barriers. The resulting $^{11}\text{BOC}_3\text{H}_4$ doublet radical intermediates underwent unimolecular decomposition involving three competing reaction mechanisms via two distinct atomic hydrogen losses and a methyl group elimination. Utilizing partially deuterated methylacetylene reactants (CD_3CCH ; CH_3CCD), we revealed that the initial addition of $^{11}\text{BO}(X^2\Sigma^+)$ to the C1 carbon atom of methylacetylene was followed by hydrogen loss from the acetylenic carbon atom (C1) and from the methyl group (C3) leading to 1-propynyl boron monoxide ($\text{CH}_3\text{CC}^{11}\text{BO}$) and propadienyl boron monoxide ($\text{CH}_2\text{CCH}^{11}\text{BO}$), respectively. Addition of $^{11}\text{BO}(X^2\Sigma^+)$ to the C1 of methylacetylene followed by the migration of the boronyl group to the C2 carbon atom and/or an initial addition of $^{11}\text{BO}(X^2\Sigma^+)$ to the sterically less accessible C2 carbon atom of methylacetylene was followed by loss of a methyl group leading to the ethynyl boron monoxide product (HCC^{11}BO) in an overall exoergic reaction ($78 \pm 23 \text{ kJ mol}^{-1}$). The branching ratios of these channels forming $\text{CH}_2\text{CCH}^{11}\text{BO}$, $\text{CH}_3\text{CC}^{11}\text{BO}$, and HCC^{11}BO were derived to be $4 \pm 3\%$, $40 \pm 5\%$, and $56 \pm 15\%$, respectively; these data are in excellent agreement with the calculated branching ratios using statistical RRKM theory yielding 1%, 38%, and 61%, respectively.



1. INTRODUCTION

During the last few decades, micrometer-sized metal powders of aluminum have been exploited as additives to solid state rocket propellants, since the oxidation of fine powdered aluminum particles releases considerably more energy than conventional hydrocarbons such as JP-8 jet fuel, that is, 837 kJ mol^{-1} versus 230 kJ mol^{-1} .¹ The lightest main group III element, boron (B), holds the highest energy density value by combustion of any element in the periodic system. At room temperature and pressure, the gravimetric and volumetric heats of oxidation of boron (58.7 kJ g^{-1} and 137.5 kJ cm^{-3}) are greater than aluminum (31.0 kJ g^{-1} and 83.7 kJ cm^{-3}).² Oxidation of boron (630 kJ mol^{-1}) produces almost three times more energy than conventional hydrocarbon based jet propellants;³ therefore, boron is considered to be a potential fuel additive to produce high energy density propellants.⁴ In spite of seeming to be the ideal “metallic” fuel to be used in solid propellants, it has rarely been exploited in jet propulsion

systems to date.² The combustion process of solid boron does not undergo full energy release during the ignition process due to a delayed and incomplete oxidation of boron because of the presence of a liquid diboron trioxide (B_2O_3) layer on the boron surface generated during the combustion of the boron particles. Further, the combustion of boron in the presence of hydrogen containing chemicals is thought to diminish the energy release due to the formation of HBO and HBO₂ transient species.⁴

Therefore, extensive studies both experimentally and theoretically have been conducted over the past several years to rationalize the ignition and combustion processes of boron.^{3,5–15} A semiempirical combustion model proposed by

Special Issue: Curt Wittig Festschrift

Received: March 20, 2013

Revised: May 6, 2013

Published: May 7, 2013

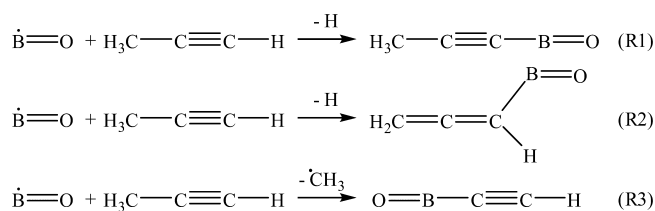
King and Kuo et al.^{6,8,14,15} and a chemical model proposed by the Princeton/Aerodyne research groups^{16–18} consider several ignition and combustion parameters, reaction mechanisms, and intermediates to probe the ignition and combustion process of boron properly. It has now been accepted that boron undergoes a two-stage combustion process. The first stage is a slow kinetic or/and diffusion controlled combustion, followed by removal of the diboron trioxide (B_2O_3) layer by vaporization at high temperatures of typically 2300 K. The second stage presents the clean combustion of the boron particle. The full energy release in combustion of boron is possible, when the final product is only B_2O_3 . However, in a hydrogen and oxygen containing environment, the energy release is limited by the formation of HBO and HBO_2 intermediates.^{2,4} Several researchers have investigated the removal of the oxide layer by introducing fluorine into the combustion environment.^{4,19–24} The ignition and combustion of boron particles is enhanced significantly in the presence of fluorine containing materials due to an optimized B_2O_3 layer removal process. Several investigations were performed in water-vapor and oxygen-rich environments as well; these demonstrated that the combustion time and oxygen concentration are inversely proportional; further, the presence of water vapor decreases the combustion time.^{25,26} Several kinetic models were developed to study the gasification of the B_2O_3 layer in a hydrocarbon environment.^{27,28} Brown et al. established a molecular level gas phase kinetics model for the combustion process of the B/O/C/H/F system.^{16–20,29,30} This model, although the most comprehensive, lacks detailed experimental input parameters such as reaction products and their kinetics. Pfitzner et al. proposed a simplified model using the kinetics model of Zhou et al. and experiments done by Kuo et al.¹⁴ Based on these studies, Pfitzner et al. expressed the requirement for accurate experimental parameters and reaction products to execute the full chemical kinetics model. Therefore, an experimental and theoretical investigation of the basic bimolecular reactions on the most fundamental, microscopic level in boron-based combustion processes becomes necessary.

In recent years, our group systematically investigated the reaction dynamics of boron atoms with unsaturated hydrocarbons such as acetylene (C_2H_2), ethylene (C_2H_4), methylacetylene (CH_3CCH), allene (CH_2CCH_2), dimethylacetylene (CH_3CCCH_3), and benzene (C_6H_6)^{31–37} to elucidate the reaction dynamics and reaction mechanisms in the B/C/H system.³⁸ However, combustion processes and the associated combustion models require the incorporation of oxygen, thus expanding to the B/C/H/O system; nevertheless, experimental studies on B/C/H/O molecules are sparse. The formation of boron monoxide (BO) during the combustion of boron was proposed,^{30,39} but the reactions of boron monoxide have never been investigated thoroughly. Further, the oxidation of boron proceeds via the successive oxidation sequence as $B \rightarrow BO \rightarrow BO_2 \rightarrow B_2O_3$ with the formation of BO as the very first step.^{30,39} Reactions of boron monoxide with molecular hydrogen and molecular oxygen were probed by focusing on the formation of HOBO/HBO and BO_3 species.^{40,41} Surprisingly, except the recent crossed molecular beam experiment of boron monoxide (BO) with the hydrocarbons acetylene (C_2H_2)⁴² and ethylene (C_2H_4)^{42,43} as investigated by our group, the reaction dynamics of boron monoxide with hydrocarbons have never been explored. Here, the reaction ^{11}BO with acetylene was probed under single collision conditions at a collision energy of 13 kJ mol^{-1} using the crossed molecular beam technique. The reaction was initiated

by an addition of the boron atom of the ^{11}BO radical to the carbon–carbon triple bond without an entrance barrier and preceded via indirect scattering dynamics by forming an $^{11}BOC_2H_2$ collision complex. The latter underwent hydrogen atom emission via a tight exit transition state to form the linear ethynyl boron monoxide molecule ($HCC^{11}BO$) in an overall exoergic ($62 \pm 8 \text{ kJ mol}^{-1}$) reaction.⁴² Successively, the authors probed the chemical dynamics of the reaction of boron monoxide with ethylene at a similar collision energy of 12 kJ mol^{-1} . The reaction also proceeded through indirect scattering dynamics leading to the formation of the doublet $^{11}BOC_2H_4$ reaction intermediate. This intermediate underwent unimolecular decomposition through hydrogen atom emission via a tight exit transition state to form a planar, C_s symmetric vinyl boron monoxide molecule (C_2H_3BO) with an overall reaction exoergicity of $42 \pm 13 \text{ kJ mol}^{-1}$.

We expand these studies of boron monoxide reactions and investigate the reaction dynamics of boron monoxide with methylacetylene (CH_3CCH) together with its partially deuterated counterparts (CD_3CCH ; CH_3CCD) in an attempt to systematically elucidate the reaction dynamics of boron monoxide with unsaturated hydrocarbon molecules under single collision reaction conditions. The present work utilizes crossed molecular beams technique along with ab initio calculations and RRKM theory to investigate the reaction dynamics and products of the title reaction. Methylacetylene (CH_3CCH ; X^1A_1) is the simplest member of an alkyl substituted acetylene. In principle, the substitution of an acetylenic hydrogen atom by a methyl group can open two additional reaction channels along with the formation of 1-propynyl boron monoxide (CH_3CCBO) (R1): the formation of propadienyl boron monoxide (CH_2CCHBO) (R2) and ethynyl boron monoxide ($HCCBO$) (R3), respectively (see Scheme 1). We will also compare the reaction dynamics of the

Scheme 1. Potential Reaction Products of the Boron Monoxide versus Atomic Hydrogen (R1/R2) and Methyl Replacement Reactions (R3)



title reaction with those of the isoelectronic reaction of cyano radicals (CN ; $X^2\Sigma^+$) with methylacetylene (CH_3CCH , X^1A_1) studied previously under single collision conditions.⁴⁴

2. EXPERIMENTAL AND DATA ANALYSIS

The reactions of the ground state boron monoxide radical (BO ; $X^2\Sigma^+$) with methylacetylene (CH_3CCH ; X^1A_1) were conducted in a universal crossed molecular beams machine under single collision conditions.^{45–49} Briefly, a supersonic beam of ground state boron monoxide (BO ; $X^2\Sigma^+$) was produced in situ via laser ablation of a boron rod at 266 nm and seeding the ablated boron in pure carbon dioxide carrier gas (CO_2 , 99.99%, BOC gases).⁵⁰ The fourth harmonic output of a Spectra-Physics Quanta-Ray Pro 270 Nd:YAG laser (266 nm) operating at a repetition rate of 30 Hz was focused with an output power of 15–20 mJ per pulse on the rotating boron rod using a lens of

1500 mm focal length. The carbon dioxide gas was released by a Proch–Trickl pulsed valve with a nozzle diameter of 1 mm operating at 60 Hz with 80 μs pulse width and -350 V pulse amplitude.⁵¹ A backing pressure of 4 atm was used, which yielded a pressure of 5×10^{-4} Torr inside the primary source chamber. The carbon dioxide reacted with the ablated boron atoms to produce $\text{BO}(X^2\Sigma^+)$ possibly via atomic oxygen abstraction; the beam passed through a skimmer of diameter 1 mm. A four-slot chopper wheel operating at a speed of 120 Hz was placed 18 mm downstream the skimmer and selected a 11.2 μs segment of the $\text{BO}(X^2\Sigma^+)$ beam with a peak velocity (v_p) of $1453 \pm 40\text{ ms}^{-1}$ and speed ratio S of 2.2 ± 0.3 .

The segment of the primary beam was crossed by a second pulsed molecular beam of methylacetylene perpendicularly in the interaction region. Methylacetylene (Scott Specialty Gases; 99%+) was released by a second Proch–Trickl pulsed valve operating at a repetition rate of 60 Hz with an 80 μs pulse width from a backing pressure of 550 Torr characterized by a peak velocity of $840 \pm 10\text{ ms}^{-1}$ and speed ratio of $S = 12.0 \pm 0.2$. The collision energy between $^{11}\text{BO}(X^2\Sigma^+)$ and methylacetylene was determined to be $22.7 \pm 1.2\text{ kJ mol}^{-1}$. Note that both pulsed valves, the laser pulse, and the chopper wheel were synchronized by three digital pulse generators (Stanford Research System, DG535) with the help of two frequency dividers (Pulse Research Lab, PRL-220A). The time zero trigger originates from a photo diode, mounted on the top of the chopper wheel. The primary and the secondary pulsed valves were triggered 1882 and 1872 μs , respectively, after the time zero trigger pulse. The laser was triggered 156 μs after the trigger pulse of the primary pulsed valve.

The ro-vibrational levels of the boron monoxide radical were characterized in situ via laser-induced fluorescence (LIF) spectroscopy.⁵² Briefly, the $^2\Sigma^+$ electronic ground state of the boron monoxide radical was probed via the $A^2\Pi-X^2\Sigma^+$ transition. The (0,0) vibrational band near 425 nm was recorded by using the Nd:YAG pumped Lambda Physik Scanmate dye laser output of 10 μJ per pulse. The spectra were analyzed using the diatomic spectral simulation program developed by Tan.⁵³ The rotational temperature was determined to be 250 K.⁵² This indicates that the ^{11}BO radicals have a maximum of 2 kJ mol^{-1} of internal energy.^{43,52} The LIF spectrum of ^{11}BO radical did not show any (1,1) vibrational band; based on the noise, less than 5% of ^{11}BO radical were suggested to reside in the $\nu = 1$ level.⁵²

The reactively scattered products were monitored using a triply differentially pumped quadrupole mass spectrometer (QMS) in the time-of-flight (TOF) mode after electron-impact ionization of the neutral species at 80 eV electron energy with an emission current of 2 mA. The extracted ions pass through the quadrupole mass filter (Extrel QC 150) operated with an oscillator frequency of 2.1 MHz. Only ions with a selected mass-to-charge (m/z) ratio pass through the quadrupole mass filter and are accelerated toward a stainless steel target coated with a thin layer of aluminum maintained at a voltage of -22.5 kV . The ions hit the surface and initiate an electron cascade until it reaches an aluminum coated organic scintillator, whose photon cascade is detected by a photomultiplier tube (PMT, Burle, model 8850) operated at -1.35 kV . The signal from the PMT was then filtered by a discriminator (Advanced Research Instruments, model F-100TD, level: 1.6 mV) prior to feeding into a multichannel scaler (Stanford Research System SR430) to record the time-of-flight spectra.^{47,49} The detector is

rotatable in the plane defined by the primary and the secondary reactant beams to allow taking angular resolved TOF spectra.

At each angle, up to 5.1×10^5 and 7.7×10^5 TOF spectra were accumulated for the atomic hydrogen and methyl loss channels, respectively, in batches of 51 200 TOF spectra. The recorded TOF spectra were then integrated and normalized to extract the product angular distribution in the laboratory frame. To gain information on the reaction dynamics, the experimental data must be transformed into the center-of-mass reference frame utilizing a forward-convolution routine.^{54,55} This iterative method assumes an initial choice of angular flux distribution, $T(\theta)$, and the product translational energy distribution, $P(E_T)$ in the center-of-mass frame. Laboratory TOF spectra and the laboratory angular distribution were then calculated from the $T(\theta)$ and $P(E_T)$ functions and were averaged over a grid of Newton diagrams to account for the apparatus functions and the beam spreads in velocity and direction. Best fits were obtained by iteratively refining the adjustable parameters in the center-of-mass functions within the experimental error limits of, for instance, peak velocity, and speed ratio, error bars in the laboratory angular distribution. The product flux contour map, $I(\theta, u) = P(u) \times T(\theta)$, reports the intensity of the reactively scattered products (I) as a function of the CM scattering angle (θ) and product velocity (u). This plot is called the reactive *differential cross section* and gives an *image* of the chemical reaction. The branching ratios of the channels were calculated using the method proposed by Krajnovich et al.⁵⁶

3. THEORETICAL CALCULATIONS

The reaction paths in the reaction of boron monoxide (BO , $X^2\Sigma^+$) with methylacetylene were also investigated computationally on the doublet surface. The geometries of all structures i.e. reactants, products, intermediates and transition states were optimized at CCSD(T)-fc^{57–60} level of theory using the cc-pVTZ^{61,62} basis set. Harmonic vibrational frequencies were computed at the same level of theory to characterize structures as minima or transition states. The connection of two minima by a transition state was determined by visual inspection of the imaginary vibrational mode. Improved energies were obtained by a composite method. SCF energies were calculated using the cc-pVQZ^{61,62} and cc-pVSZ^{61,62} basis sets and were extrapolated with the empirical factor of Schwenke.⁶³ CCSD(T)-fc energies were calculated with the cc-pVTZ and cc-pVQZ basis sets and the CCSD and (T) correlation energies were extrapolated with the empirical scheme of Bakowies⁶⁴ and the empirical factor of Schwenke,⁶³ respectively. To account for higher correlation effects, the correlation energy difference between CCSDT-fc/cc-pVDZ^{61,62,65–67} and CCSD(T)-fc/cc-pVDZ was computed. Core polarization and correlation effects were calculated by computing the energy difference between CCSD(T)/cc-pCVTZ^{61,62} and CCSD(T)-fc/cc-pVTZ. The compound energies were obtained by adding the two extrapolated energies, the two energy differences, spin–orbit coupling energy and the scaled zero point vibrational energy (ZPE). We have chosen to scale the ZPE by 0.99. This factor is derived from a thorough study of scaling factors⁶⁸ for ZPEs, fundamental frequencies, and other properties related to vibrational frequencies. We observe that the scaling factors for fundamental frequencies for MP2/6-311+G(d,p) and MP2/cc-pVTZ are quite similar. Therefore we take the scaling factor for zero-point vibrational energies for CCSD(T)/6-311+G(d,p) to be appropriate for CCSD(T)/cc-pVTZ, too. In a test

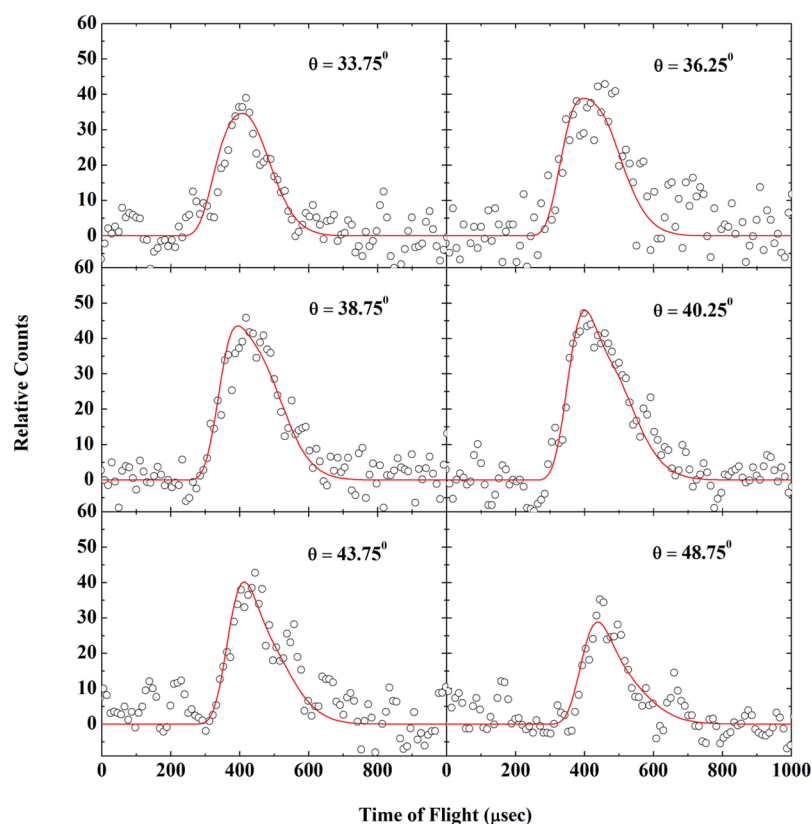


Figure 1. Time-of-flight data recorded at $m/z = 66$ ($^{11}\text{BOC}_3\text{H}_3^+$) at various angles for the reaction between boron monoxide (^{11}BO ; $X^2\Sigma^+$) with methylacetylene (CH_3CCH ; X^1A_1) at a collision energy of 22.7 ± 1.2 kJ mol^{-1} . The circles indicate the experimental data, and the solid lines indicate the calculated fit.

against total atomization energies (TAEs) from the Active Thermochemical Tables,^{69–71} (as given in ref 72) this composite method reproduced heats of reaction where bonds between first row atoms change with a mean signed error of 0.2 kJ mol^{-1} and a standard deviation of 1.2 kJ mol^{-1} . The largest error was 1.6 kJ mol^{-1} . Our molecules are approximately three times as large as those in the test set. Therefore we assume the standard deviation in compound energies to be 4 kJ mol^{-1} . The corresponding error bar for a 95% confidence level is approximately 2.5 times as large, resulting in a ± 9 kJ mol^{-1} uncertainty. Electronic structure calculations used the ACES II program.⁷³ In a few cases, we used NWChem 6.1^{74,75} to calculate CCSDT energies, and in one case we used Cfour⁷⁶ to analytically calculate harmonic vibrational frequencies.

Besides the stationary points, we also attempted to predict the branching ratios of the products utilizing Rice–Ramsperger–Kassel–Marcus (RRKM) theory. Here, the rate constant (k) for a reaction $A^* \rightarrow A^\ddagger \rightarrow P$ (where A^* is the energized reactant, \ddagger is the transition state, and P is the product) may be expressed via eq 1:^{77,78}

$$k(E) = \frac{\sigma W^\ddagger(E - E^\ddagger)}{h \rho(E)} \quad (1)$$

In this equation E and E^\ddagger are the energies of reactant and transition state, σ is the symmetry factor, h is Planck's constant, $W^\ddagger(E - E^\ddagger)$ is the number of states of the transition state, and $\rho(E)$ is the density of states of the reactant. ρ and W^\ddagger were computed by the saddle point method. Molecules were treated as collections of harmonic oscillators.⁷⁹ In this model, the symmetry factor is identical to the degeneracy of the reaction

path. Tunneling corrections are computed by the Eckart formula.^{80,81} Rate constants were computed using relative energies determined with the compound method. We calculated rate constants with the program RRKM_01.^{82,83} To calculate branching ratios (as quotients of product concentrations at infinite time), we used BRANCH.^{82,83}

4. RESULTS

4.1. Laboratory Data. A reactive scattering signal for the reaction of boron monoxide ($^{11}\text{BO}(X^2\Sigma^+)$ (27 amu) with methylacetylene (CH_3CCH , X^1A_1) (40 amu) was recorded at mass-to-charge ratios of $m/z = 66$ ($^{11}\text{BOC}_3\text{H}_3^+$) and $m/z = 65$ ($^{11}\text{BOC}_3\text{H}_2^+ / ^{10}\text{BOC}_3\text{H}_3^+$) for the atomic hydrogen and/or molecular hydrogen loss pathways, respectively; a further signal was taken at $m/z = 52$ ($^{11}\text{BOC}_2\text{H}^+$) to probe the methyl group (CH_3) loss channel (Figures 1 and 2). After scaling, the TOF spectra at $m/z = 66$ and $m/z = 65$ depicted an identical profile. These observations indicate that the ions at $m/z = 65$ originated from the dissociative ionization of the $^{11}\text{BOC}_3\text{H}_3$ parent (66 amu) in the electron impact ionizer of the detector. Therefore, we can conclude that in the reaction of $^{11}\text{BO}(X^2\Sigma^+)$ with methylacetylene (CH_3CCH , X^1A_1), the boron monoxide versus atomic hydrogen loss channel leading to the formation of $^{11}\text{BOC}_3\text{H}_3$ isomer(s) is open; further, the molecular hydrogen loss channel is found to be closed and/or below our detection limit. The TOF spectra recorded at $m/z = 52$ (methyl loss channel) are distinctly different from those TOF spectra obtained at $m/z = 66$ (atomic hydrogen loss). Therefore, we can conclude from the raw data that the TOF spectra recorded at $m/z = 52$ do not originate from dissociative

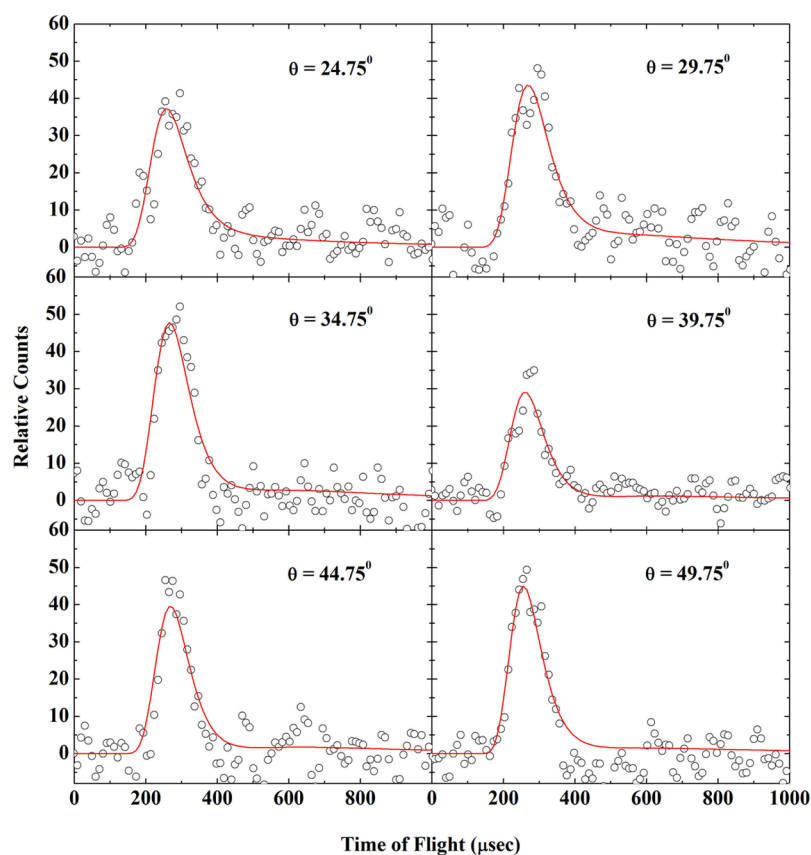


Figure 2. Time-of-flight data recorded at $m/z = 52$ ($^{11}\text{BOC}_2\text{H}^+$) at various angles for the reaction between boron monoxide (^{11}BO ; $X^2\Sigma^+$) with methylacetylene (CH_3CCH ; X^1A_1) at a collision energy of 22.7 ± 1.2 kJ mol^{-1} . The circles indicate the experimental data, and the solid lines indicate the calculated fit.

ionization of the $^{11}\text{BOC}_3\text{H}_3$ parent in the electron impact ionizer but likely from the methyl loss channel.

In the case of the atomic hydrogen loss, the fits of the TOF spectra and of the laboratory angular distribution were carried out with a single channel fit and a product mass combination of 66 amu ($^{11}\text{BOC}_3\text{H}_3$) and 1 amu (H). Note that the laboratory angular distribution was obtained by integrating the TOF spectra taken for the $^{11}\text{BOC}_3\text{H}_3$ product at $m/z = 66$ (Figure 3). Here, the angular distribution extends at least 45.0° in the scattering plane defined by the primary and the secondary molecular beams and peaks at $39.0 \pm 0.5^\circ$ close to the center-of-mass (CM) angle of $40.5 \pm 1.0^\circ$. The nearly symmetric laboratory angular distribution around the center-of-mass angle suggests that the reaction proceeds via indirect (complex forming) scattering dynamics involving $^{11}\text{BOC}_3\text{H}_4$ reaction intermediate(s). Considering the methyl loss channel (Figures 2 and 4), both the TOF and the laboratory angular distribution were fitted with a single channel and a product mass combination of 52 amu ($^{11}\text{BOC}_2\text{H}$) and 15 amu (CH_3). The laboratory angular distribution is shown in Figure 4 for the heavy reaction product at 52 amu ($^{11}\text{BOC}_2\text{H}$). As expected from the significantly enhanced scattering range due to the product mass combination of 52 and 15 amu and the reaction exoergicity, the laboratory angular distribution is very broad, and products are scattered over a wide angular range, that is, of about 205° based on the Newton diagrams.

Having identified two distinct exit channels, that is, the atomic hydrogen and methyl loss pathways, we are focusing our attention now on the position of the atomic hydrogen loss.

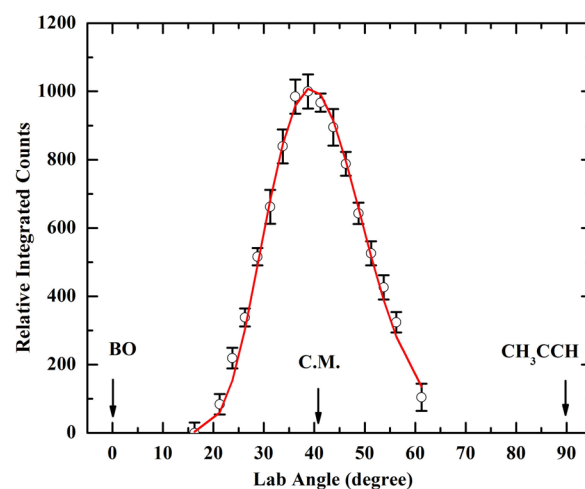


Figure 3. Laboratory angular distribution (LAB) of $^{11}\text{BOC}_3\text{H}_3^+$ ions ($m/z = 66$) recorded for the reaction of boron monoxide (^{11}BO ; $X^2\Sigma^+$) with methylacetylene (CH_3CCH ; X^1A_1) at a collision energy of 22.7 ± 1.2 kJ mol^{-1} . The circles and error bars indicate the experimental data, and the solid line indicates the calculated distribution.

Recall that, in the methylacetylene reactant, the hydrogen atoms at the acetylenic and methyl group are chemically nonequivalent. Therefore, we utilized partially deuterated reactants (CD_3CCH and CH_3CCD) to elucidate the position of the atomic hydrogen loss. First, we carried out the reaction of D3-methylacetylene, $\text{CD}_3\text{CCH}(X^1A_1)$, with $^{11}\text{BO}(X^2\Sigma^+)$. A

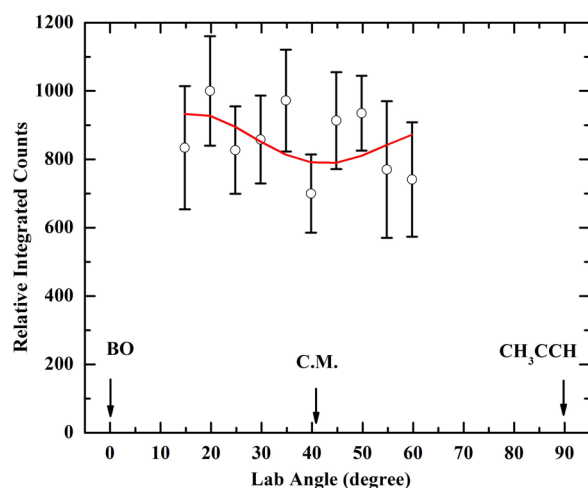


Figure 4. Laboratory angular distribution (LAB) of $^{11}\text{BOC}_2\text{H}^+$ ions ($m/z = 52$) recorded for the reaction of boron monoxide (^{11}BO ; $X^2\Sigma^+$) with methylacetylene (CH_3CCH ; X^1A_1) at a collision energy of $22.7 \pm 1.2 \text{ kJ mol}^{-1}$. The circles and error bars indicate the experimental data, and the solid line indicates the calculated distribution.

hydrogen loss can occur only from the acetylenic group and would lead to a $^{11}\text{BOC}_3\text{D}_3$ product of 69 amu. Figure 5 depicts

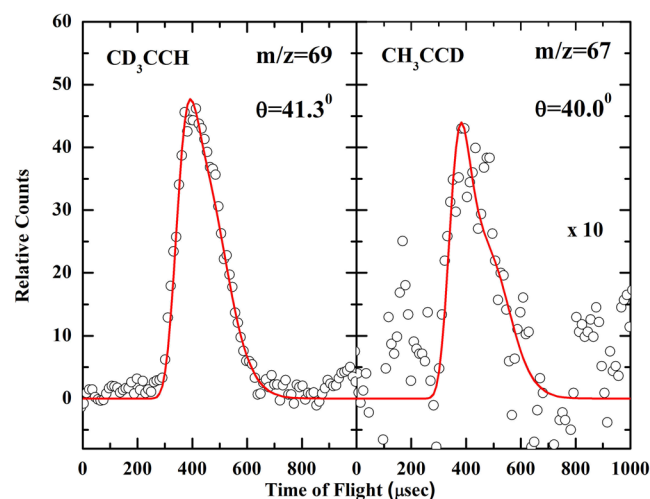


Figure 5. Time-of-flight data at the center-of-mass angles recorded for the atomic hydrogen loss pathway in the reaction of boron monoxide (^{11}BO ; $X^2\Sigma^+$) with D3-methylacetylene (CD_3CCH ; X^1A_1) (left) and D1-methylacetylene (CH_3CCD ; X^1A_1) at $m/z = 69$ ($^{11}\text{BOC}_3\text{D}_3^+$) and $m/z = 67$ ($^{11}\text{BOC}_3\text{H}_2\text{D}^+$), respectively.

the corresponding TOF spectra at the center-of-mass angle recorded at $m/z = 69$, that is, $^{11}\text{BOC}_3\text{D}_3^+$. This finding clearly confirms the existence of the atomic hydrogen loss channel from the acetylenic group. Second, we explored a potential atomic hydrogen ejection from the methyl group. For this, we conducted the crossed beam reaction of D1-methylacetylene, CH_3CCD (X^1A_1), with $^{11}\text{BO}(X^2\Sigma^+)$; a hydrogen loss from the methyl group should lead to the formation of a $^{11}\text{BOC}_3\text{H}_2\text{D}$ product with a mass of 67 amu. Note that a competing atomic deuterium loss does not interfere, since this channel leads to the formation of $^{11}\text{BOC}_3\text{H}_3$ product holding a mass of only 66 amu. As evident from Figure 5, signal of $^{11}\text{BOC}_3\text{H}_2\text{D}^+$ ions was recorded at $m/z = 67$ at the center-of-mass angle. Therefore,

the TOF spectra taken at $m/z = 67$ confirms the presence of a weaker hydrogen atom loss channel from the methyl group of methylacetylene. Note that for both partially deuterated methylacetylene, we recorded the TOF spectra only at the center-of-mass angle because of low signal counts and the high cost of these chemicals. An integration of these TOF spectra indicates fractions of the hydrogen loss from acetylenic versus methyl group of about 90% versus 10% (assuming the similar ionization efficiency of both the products).

4.2. Center-of-Mass System. **4.2.1. Center-of-Mass Translational Energy Distributions.** To elucidate the chemical dynamics of the boron monoxide–methylacetylene system, the laboratory data are transformed into the center-of-mass reference frame utilizing a forward convolution routine as described in Section 2. The corresponding center-of-mass angular and translational energy distributions are shown in Figures 6 and 7 for both the atomic hydrogen and methyl loss

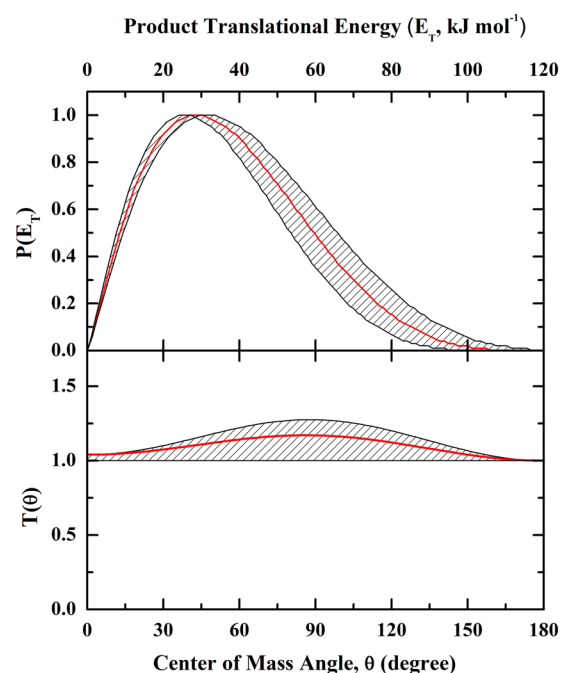


Figure 6. Center-of-mass translational energy distribution (top) and center-of-mass angular distribution (bottom) for the atomic hydrogen loss pathway in the reaction between boron monoxide (^{11}BO ; $X^2\Sigma^+$) with methylacetylene (CH_3CCH ; X^1A_1) leading to $^{11}\text{BOC}_3\text{H}_3$ isomers. The hatched areas indicate the acceptable lower and upper limits of the fits, and the solid red line defines the best-fit functions.

pathways, respectively. Let us focus on the atomic hydrogen loss first. Figure 6 (top) presents the center-of-mass translational energy distribution, $P(E_T)$, obtained for the $^{11}\text{BOC}_3\text{H}_3$ plus atomic hydrogen channel; this distribution depicts a maximum translational energy release, E_{max} of $105 \pm 15 \text{ kJ mol}^{-1}$. For those product molecules formed without internal excitation, the maximum translational energy release presents the sum of the collision energy plus the reaction exoergicity. Therefore, the exoergicity of the hydrogen loss channel can be extracted by subtracting the collision energy ($22.7 \pm 1.2 \text{ kJ mol}^{-1}$) from the maximum translational energy ($105 \pm 15 \text{ kJ mol}^{-1}$). This leads to a reaction exoergicity of $82 \pm 16 \text{ kJ mol}^{-1}$ to form $^{11}\text{BOC}_3\text{H}_3$ isomer(s) plus atomic hydrogen. Further, the translational energy flux distribution is displaced from zero translational energy and shows a distribution maximum

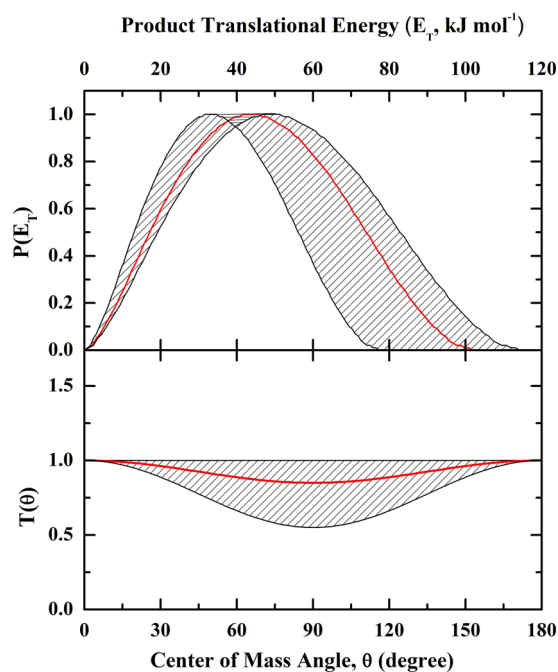


Figure 7. Center-of-mass translational energy distribution (top) and center-of-mass angular distribution (bottom) for the methyl loss pathway in the reaction between boron monoxide (^{11}BO ; $X^2\Sigma^+$) with methylacetylene (CH_3CCH ; X^1A_1) leading to HCC^{11}BO isomer(s). The hatched areas indicate the acceptable lower and upper limits of the fits, and the solid red line defines the best fit functions.

between 20 and 35 kJ mol^{-1} . This suggests the presence of an exit barrier and hence a tight exit transition state when the $^{11}\text{BOC}_3\text{H}_4$ intermediate decomposes to the product(s).⁸⁴ This exit transition state (repulsive bond rupture) involves a significant electron rearrangement. Finally, the center-of-mass translational energy distribution allows us to determine the average amount of energy released into the translational degrees of freedom of the products, that is, $36 \pm 7\%$ of the total available energy.

In case of the methyl loss channel (Figure 7), the center-of-mass translational energy distribution portrays a maximum translational energy release of $101 \pm 22 \text{ kJ mol}^{-1}$, which translates into a reaction exoergicity of the HCC^{11}BO plus CH_3 channel of $78 \pm 23 \text{ kJ mol}^{-1}$ after subtracting the collision energy. Additionally, the maximum of the flux distribution

peaks significantly away from zero translational energy between 30 and 50 kJ mol^{-1} also indicating the presence of a tight exit transition state. Finally, the fraction of available energy channeling into the translational degrees of freedom of the products on average was calculated to be $46 \pm 11\%$.

4.2.2. Center-of-Mass Angular Distributions. The center-of-mass angular distributions, $T(\theta)$'s, deliver additional information on the chemical dynamics of the title reaction; they are portrayed in Figures 6 and 7 for the atomic hydrogen and methyl loss pathways, respectively. Both distributions show intensities over the whole angular range from 0° to 180° ; this finding is indicative of indirect scattering dynamics involving the formation of $^{11}\text{BOC}_3\text{H}_4$ collision complexes for both the atomic hydrogen and methyl loss pathways.⁸⁵ Further, both distributions are essentially forward–backward symmetric with respect to 90° . This forward–backward symmetry proposes that the lifetime of the decomposing $^{11}\text{BOC}_3\text{H}_4$ complexes, which emit the hydrogen atom and the methyl group, is longer than their rotation periods.⁸⁵ Despite these similarities, the hydrogen and methyl loss pathways hold a striking difference. Whereas for the atomic hydrogen loss pathway, the best fit $T(\theta)$ depicts a slight distribution *maximum* at 90° , the $T(\theta)$ for the methyl loss pathway shows a *minimum* at 90° . These findings infer geometrical constraints in the exit channels.⁸⁵ Considering the atomic hydrogen loss, the hydrogen atom is suggested to be emitted almost perpendicularly to the plane of the decomposing $^{11}\text{BOC}_3\text{H}_4$ complex, that is, nearly parallel to the total angular momentum vector; on the other hand, the methyl group is lost preferentially within the plane of the fragmenting $^{11}\text{BOC}_3\text{H}_4$ complex, that is, almost perpendicularly to the total angular momentum vector.⁸⁵ These findings are also compiled in the flux contour maps (Figure 8).

We have also analyzed the branching ratios of the product channels.⁵⁶ The branching ratios for both hydrogen atom loss channels R1 ($\text{CH}_3\text{CC}^{11}\text{BO}$) and R2 ($\text{CH}_2\text{CCH}^{11}\text{BO}$) together with the methyl loss pathway R3 (HCC^{11}BO) as shown in Scheme 1, were calculated to be $40 \pm 5\%$: $4 \pm 3\%$: $56 \pm 15\%$. Note that to derive the branching ratios of the hydrogen loss from the methyl versus acetylenic carbon atom, data from the crossed beam reactions with D3- and D1-methylacetylene were analyzed quantitatively (Section 4.1).

5. THEORETICAL RESULTS

We also investigate the title reaction computationally (Figures 9 and 10; Supporting Information). These calculations predict

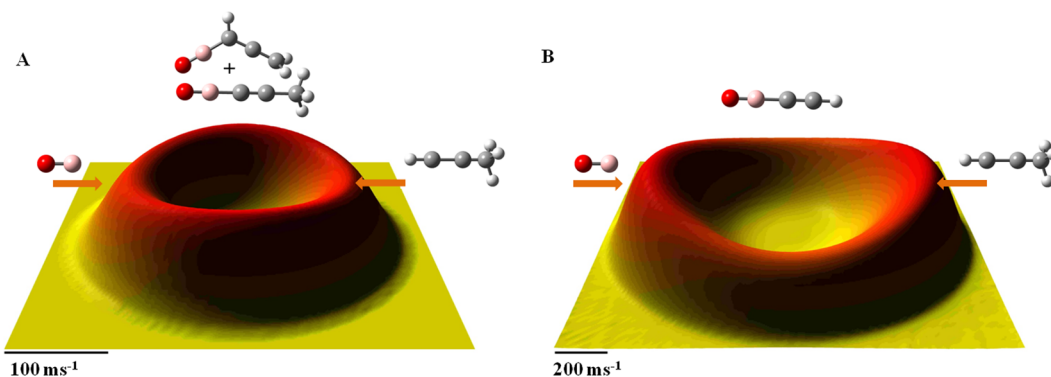


Figure 8. Flux contour maps of the competitive atomic hydrogen (left) and methyl loss (right) pathways in the crossed beam reaction of boron monoxide radicals with methylacetylene leading to the formation of 1-propynyl boron monoxide ($\text{CH}_3\text{CC}^{11}\text{BO}$) and propadienyl boron monoxide ($\text{CH}_2\text{CCH}^{11}\text{BO}$) (hydrogen elimination) and ethynyl boron monoxide (HCC^{11}BO) (methyl elimination).

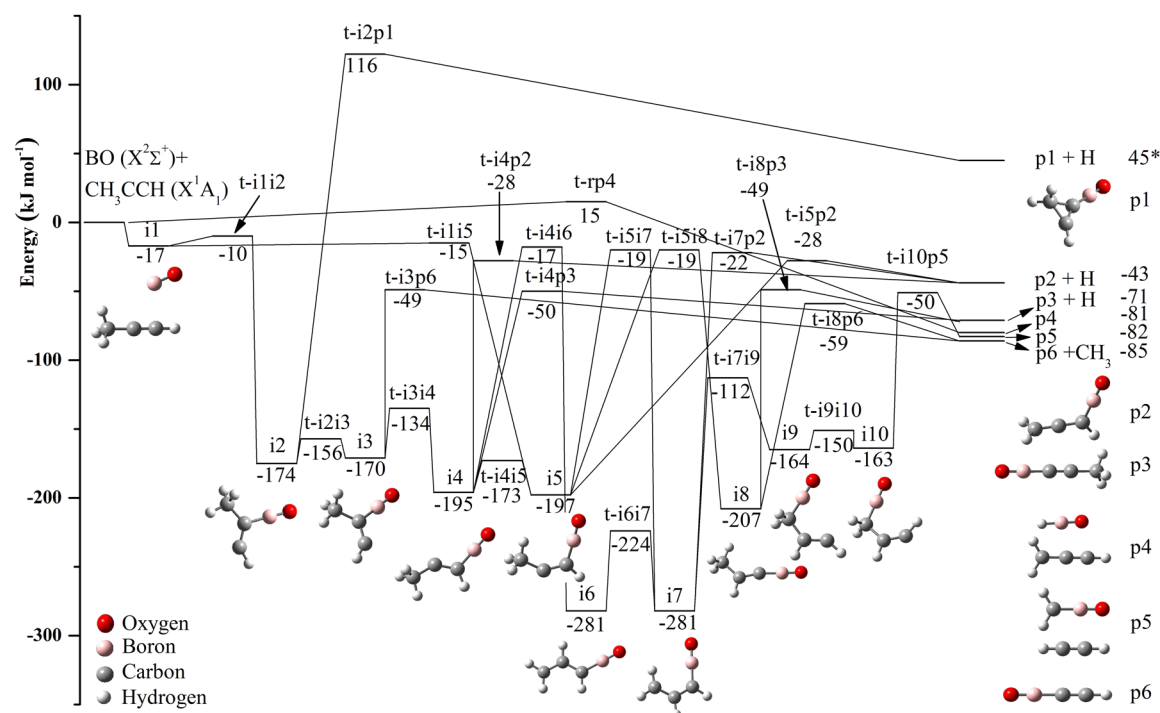


Figure 9. Schematic representation of the computed $^{11}\text{BOC}_3\text{H}_4$ potential energy surface. Corrected relative energies using composite method are given in kJ mol^{-1} (* indicates relative energies without correction).

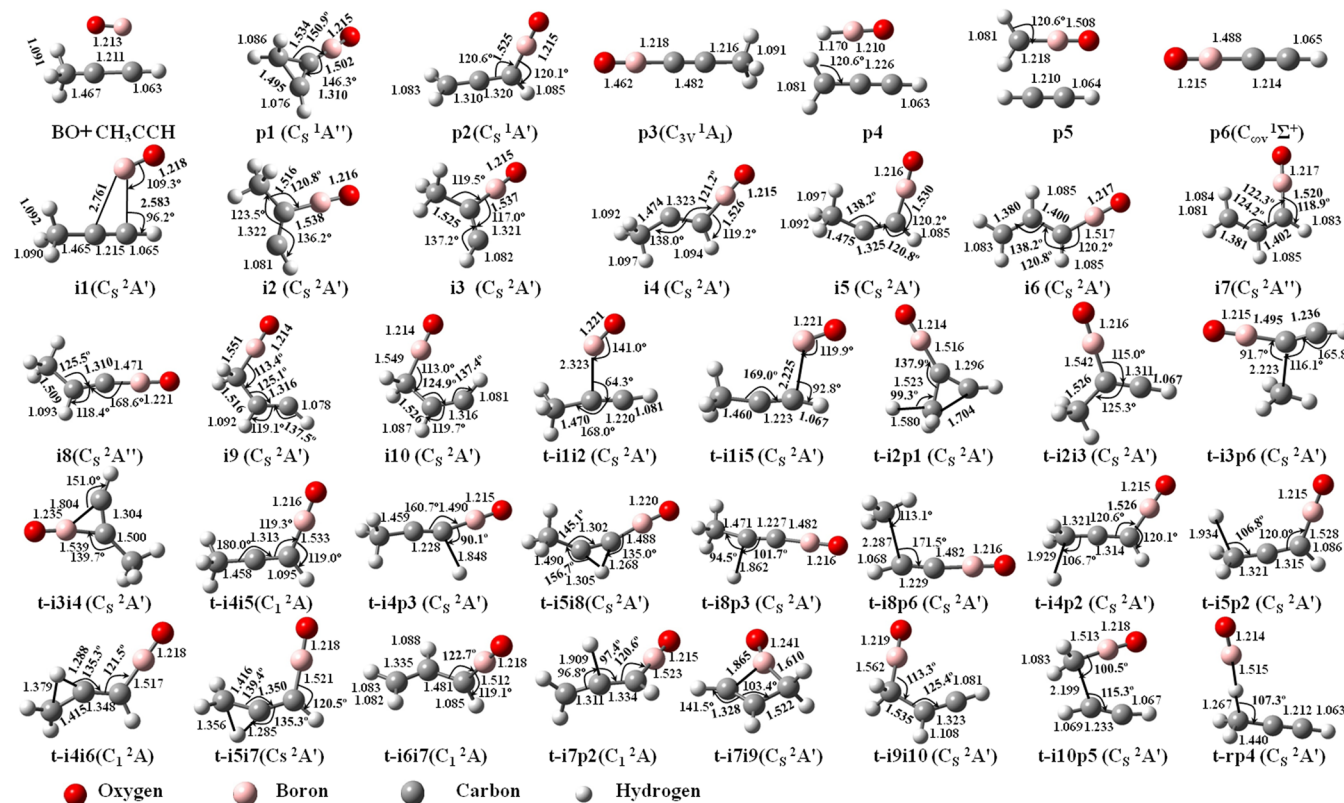


Figure 10. Structures of relevant stationary points (products, intermediates, and transition states) on the $^{11}\text{BOC}_3\text{H}_4$ potential energy surface (PES). Angles and bond lengths are shown in degrees and angstroms, respectively.

the existence of ten $^{11}\text{BOC}_3\text{H}_4$ reaction intermediates (i1–i10) and of six potential product channels (p1–p6) (Cartesian coordinates are listed in the Supporting Information). In detail, the approach of the ^{11}BO radical toward the π electron density

of the acetylenic $\text{C}\equiv\text{C}$ triple bond leads to the formation of intermediate i1 ($^{11}\text{BOC}_3\text{H}_4$) without any entrance barrier; this weakly bound intermediate can be considered as a weakly bound complex of the reactants that is 17 kJ mol^{-1} more stable

than the separated methylacetylene and boron monoxide reactants. This intermediate can undergo two isomerization pathways: the ^{11}BO radical can add to the C2 or to the C1 carbon atom of the methylacetylene reactant leading to intermediates **i2** (-174 kJ mol^{-1}) and **i5** (-197 kJ mol^{-1}), respectively. The associated barriers to addition of 7 and 2 kJ mol^{-1} , respectively, are below the energy of the separated reactants, hence indicating the existence of two submerged barriers in the entrance channel.

Structures **i2** and **i5** are interconnected via intermediates **i3** and **i4** via low barriers between 18 and 61 kJ mol^{-1} . The rate constant calculation (Supporting Information) proposes that all intermediates **i2**–**i5** are rapidly accessible. These intermediates can undergo five unimolecular decomposition pathways. First, **i2** can lose a hydrogen atom leading to a cyclic $^{11}\text{BOC}_3\text{H}_3$ product **p1**; the overall reaction to form **p1** and atomic hydrogen from the reactants is strongly endoergic by 45 kJ mol^{-1} . Second, intermediate **i3** can eliminate a methyl group leading to ethynyl boron monoxide (HCC^{11}BO) (**p6**); this channel proceeds through a tight exit transition state located $36 \pm 9 \text{ kJ mol}^{-1}$ above the separated products; it further presents the most exoergic reaction pathway ($-85 \pm 9 \text{ kJ mol}^{-1}$). Third, intermediate **i4** depicts two competing hydrogen loss pathways via tight exit transition states (15 and 21 kJ mol^{-1} above the energy of the separated products) leading to the $^{11}\text{BOC}_3\text{H}_3$ isomers **p2** (propadienyl boron monoxide; $\text{CH}_2\text{CCH}^{11}\text{BO}$) and **p3** (1-propynyl boron monoxide; $\text{CH}_3\text{CC}^{11}\text{BO}$). Both reactions are exoergic with respect to the separated reactants by 43 and 71 kJ mol^{-1} , respectively. Finally, intermediate **i5** emits atomic hydrogen through a tight exit transition state leading to **p2** (propadienyl boron monoxide; $\text{CH}_2\text{CCH}^{11}\text{BO}$).

Besides the hydrogen and methyl loss pathways, intermediates **i2**–**i5** can also isomerize via (multiple) hydrogen shifts leading eventually to intermediates **i6**–**i10**. However, the inherent transition states are very high in energy and require up to 180 kJ mol^{-1} to be overcome; this places these transition states only 15–21 kJ mol^{-1} below the energy of the separated reactants. Compared to the hydrogen/methyl loss pathways from **i2** to **i5**, the significantly higher barriers for the hydrogen shifts propose that based on these energetics alone, intermediates **i6**–**i10** should be of minor importance for the reaction mechanism; **i2**–**i5** are expected to undergo unimolecular decomposition rather than hydrogen migration to **i6**–**i10**.

The formation of acetylene (C_2H_2) and methylene boron monoxide (CH_2BO) radical (**p5**) from intermediate **i10** is uncertain due to the following two reasons: first, none of the products can be detected in our present experiment due to significant background counts at $m/z = 26$ and $m/z = 41$ from primary beam (^{10}BO) and secondary beam (^{13}C isotopically labeled methylacetylene) respectively; second, this channel has a negligible contribution due to the significantly higher barriers toward intermediate **i6**–**i10**. These conclusions are also confirmed by the rate constants obtained from our statistical calculations. Note that we also consider the addition of the boron monoxide radical with its oxygen atom to methylacetylene. However, the corresponding intermediates such as the one formed via addition of the boron monoxide with its oxygen atom to the C1-position of methylacetylene are too high in energy to be accessible under our experimental conditions (CCSD(T)-fc/cc-pVDZ: 101 kJ mol^{-1}). Since this energy is significantly higher than the collision energy of $22.7 \pm 1.2 \text{ kJ mol}^{-1}$ in our experiment, this reaction pathway is not

open under our experimental conditions and, hence, not further considered.^{42,43}

Finally, we investigate the direct hydrogen abstraction pathway from methylacetylene forming the HBO molecule and the propargyl radical (H_2CCCH , **p4**). The transition state for this pathway is higher in energy than the reactants by 15 kJ mol^{-1} . Based on the barrier-less formation of the weakly bound complex **i1**, the abstraction pathway should be energetically nonfavorable.

The computations enable predicting the branching ratios for the products. The branching ratios of the **p2** ($\text{CH}_2\text{CCH}^{11}\text{BO}$), **p3** ($\text{CH}_3\text{CC}^{11}\text{BO}$), and **p6** (HCC^{11}BO) are calculated to be 1%, 38%, and 61% respectively at a collision energy of 22.7 kJ mol^{-1} . Note that the rate constants predict that the reaction products should be formed almost exclusively from intermediates **i2** to **i5**. Lastly, due to the background from elastically scattered ^{13}C -methylacetylene $^{13}\text{CC}_2\text{H}_4$ (41 amu), the experiment is unable to probe the acetylene (C_2H_2)–methylene boron monoxide ($\text{CH}_2^{11}\text{BO}$; 41 amu) channel (**p5**), which would be accessible via the unimolecular decomposition of intermediate **i10**.

6. DISCUSSION

In order to investigate the underlying pathways and reaction dynamics for the reaction of boron monoxide radicals with methylacetylene, we correlate the experimental results with the theoretical data. Let us summarize the experimental results (R1–R5) first.

(R1) The boron monoxide–methylacetylene experiments suggest the existence of two competing reaction pathways: an atomic hydrogen loss and a methyl group elimination channel leading to $^{11}\text{BOC}_3\text{H}_3$ (66 amu) and $^{11}\text{BOC}_2\text{H}$ (52 amu) isomer(s), respectively, with relative fractions of $44 \pm 8\%$ and $56 \pm 15\%$, respectively.

(R2) Experiments of boron monoxide with D1- and D3-methylacetylene clearly depict two distinct hydrogen atom loss pathways from the acetylenic and methyl group leading to the formation of $^{11}\text{BOC}_3\text{D}_3$ (69 amu) and $^{11}\text{BOC}_3\text{H}_2\text{D}$ (67 amu) isomers, respectively, with fractions of $90 \pm 5\%$ and $10 \pm 5\%$, via atomic hydrogen versus boron monoxide exchange channels.

(R3) The center-of-mass angular distributions of the atomic hydrogen and methyl losses indicate indirect scattering dynamics via long-lived $^{11}\text{BOC}_3\text{H}_4$ complex(es). Further, both channels portray geometrical constraints with the hydrogen atom and methyl group emitted almost parallel and perpendicularly to the total angular momentum vector, that is, perpendicularly and within the rotational plane of the decomposing $^{11}\text{BOC}_3\text{H}_4$ complex(es).

(R4) The reaction energies to form $^{11}\text{BOC}_3\text{H}_3$ (66 amu) and $^{11}\text{BOC}_2\text{H}$ (52 amu) isomers plus atomic hydrogen and the methyl group are determined to be $82 \pm 16 \text{ kJ mol}^{-1}$ and $78 \pm 23 \text{ kJ mol}^{-1}$, respectively.

(R5) Both the atomic hydrogen and methyl loss pathways involve tight exit barriers in the order of 20–35 and 30–50 kJ mol^{-1} , respectively, with fractions of the available energy channeling into the translational degrees of freedom on average of $36 \pm 7\%$ and $46 \pm 11\%$, respectively.

As a first step, we are merging the experimental and computational data to identify the $^{11}\text{BOC}_3\text{H}_3$ (66 amu) and $^{11}\text{BOC}_2\text{H}$ (52 amu) isomer(s) formed in the atomic hydrogen and methyl loss channels, respectively. The calculations predict

that three distinct $^{11}\text{BOC}_3\text{H}_3$ isomers (**p1**, **p2**, **p3**) can be formed. Among them, the cyclic isomer **p1** is energetically not accessible considering the computed, overall reaction endoergicity of $45 \pm 17 \text{ kJ mol}^{-1}$, and the experimental collision energy of only $22.7 \pm 1.2 \text{ kJ mol}^{-1}$. Therefore, we can exclude **p1** from further discussion. The formation of both remaining $^{11}\text{BOC}_3\text{H}_3$ isomers **p2** (propadienyl boron monoxide; $\text{CH}_2\text{CCH}^{11}\text{BO}$) and **p3** (1-propynyl boron monoxide; $\text{CH}_3\text{CC}^{11}\text{BO}$) are associated with computed reaction exoergicities of $43 \pm 9 \text{ kJ mol}^{-1}$ and $71 \pm 9 \text{ kJ mol}^{-1}$, respectively. Within the error limits, the experimentally derived reaction exoergicity of the atomic hydrogen loss channel of $82 \pm 16 \text{ kJ mol}^{-1}$ agrees nicely with the computed reaction energy leading to the formation of the 1-propynyl boron monoxide ($\text{CH}_3\text{CC}^{11}\text{BO}$) ($-71 \pm 9 \text{ kJ mol}^{-1}$). Therefore, we can conclude that at least the 1-propynyl boron monoxide isomer **p3** ($\text{CH}_3\text{CC}^{11}\text{BO}$) is formed. This conclusion also gains support from the boron monoxide–D3-methylacetylene reaction. Here, the experimental data suggest that the acetylenic hydrogen atom is replaced by the boron monoxide reactant leading ultimately to the 1-propynyl boron monoxide isomer **p3** ($\text{CH}_3\text{CC}^{11}\text{BO}$) as a dominating $^{11}\text{BOC}_3\text{H}_3$ isomer. Recall that the experiments within the boron monoxide–D1-methylacetylene system also indicate that to a minor amount ($10 \pm 5\%$), the hydrogen atom is lost from the methyl group. A comparison of the structures of the reactants and of the $^{11}\text{BOC}_3\text{H}_3$ isomer **p2** proposes that the boronyl group can be incorporated at the C1 carbon atom followed by hydrogen loss from the C3 carbon atom yielding ultimately to the formation of the propadienyl boron monoxide ($\text{CH}_2\text{CCH}^{11}\text{BO}$) isomer (**p2**). Therefore, considering the atomic hydrogen loss pathways, we can conclude that both the 1-propynyl boron monoxide ($\text{CH}_3\text{CC}^{11}\text{BO}$; **p3**) and the propadienyl boron monoxide ($\text{CH}_2\text{CCH}^{11}\text{BO}$; **p2**) isomers are formed with 1-propynyl boron monoxide dominating over propadienyl boron monoxide with fractions of $90 \pm 5\%$ and $10 \pm 5\%$.

We are turning our attention now to the methyl loss pathway and the formation of the $^{11}\text{BOC}_2\text{H}$ (52 amu) isomer(s). Here, the computations predict the synthesis of a single isomer, that is, ethynyl boron monoxide product (HCC^{11}BO) (**p6**) with an overall reaction exoergicity of $85 \pm 9 \text{ kJ mol}^{-1}$; these data correlate very nicely with the experimentally derived reaction energy of $-78 \pm 23 \text{ kJ mol}^{-1}$. Therefore, we can conclude that the ethynyl boron monoxide product (HCC^{11}BO) (**p6**) presents the only $^{11}\text{BOC}_2\text{H}$ isomer formed in the boron monoxide versus methyl exchange pathway.

Having identified three distinct reaction products based on the energetics of the reaction and results from reactions utilizing D1- and D3-methylacetylene reactants, that is, 1-propynyl boron monoxide ($\text{CH}_3\text{CC}^{11}\text{BO}$; **p3**), propadienyl boron monoxide ($\text{CH}_2\text{CCH}^{11}\text{BO}$; **p2**), and ethynyl boron monoxide product (HCC^{11}BO ; **p6**) with experimental branching ratios of $40 \pm 5\%$, $4 \pm 3\%$, and $56 \pm 15\%$, we are proposing now the underlying reaction dynamics. A comparison of the molecular structures of the reactants with those of the reaction products **p2**, **p3**, and **p6** strongly proposes that the reaction follows indirect scattering dynamics and is initiated by a de facto addition of the boron monoxide radical with its radical center located at the boron atom to the C1 and possibly the C2 carbon atom of the methylacetylene reactant leading to intermediates **i5** and **i2**, respectively. Note that our experiments are not sensitive to the barrierless formation of the weakly bound van-der-Waals complex **i1**, which essentially isomerizes

to **i5** and **i2**. Considering the inherent barriers to addition of 2 and 7 kJ mol^{-1} , the formation of intermediate **i5** is likely preferred over **i2**. This is also supported by the enhanced cone of acceptance of the boron monoxide radical to methylacetylene at the C1 carbon atom compared to C2 due to the screening effect of the methyl group attached to the C2 atom. However, both intermediates can be easily interconverted through intermediates **i3** and **i4**. Intermediate **i4** can decompose essentially to the dominating reaction product 1-propynyl boron monoxide **p3** ($\text{CH}_3\text{CC}^{11}\text{BO}$). The computations suggest a tight exit transition state located 21 kJ mol^{-1} above the energy of the separated products. These data correlate very well with the experimental finding of a tight exit transition state suggested to reside about $20\text{--}35 \text{ kJ mol}^{-1}$ above the separated products. The existence of an exit barrier from intermediates **i4** to **p3** (21 kJ mol^{-1}) is sensible as the reversed reaction; that is, the hydrogen atom addition to a closed shell, acetylenic carbon–carbon triple bond, is associated with an entrance barrier. Further, the calculated geometry of the transition state (**t-i4p3**, Figure 10) connecting **i4** and **p3** suggests a direction of the atomic hydrogen emission almost perpendicular (90.1°) to the molecular plane. This geometry was predicted based on the detailed shape of the center-of-mass angular distribution of the atomic hydrogen loss pathway. Further, the intermediate **i4/i5** can undergo unimolecular decomposition via atomic hydrogen loss yielding the propadienyl boron monoxide ($\text{CH}_2\text{CCH}^{11}\text{BO}$; **p2**) isomer; the associated transition state is less tight and resides only 15 kJ mol^{-1} above the separated products. Therefore, we can conclude that the unimolecular decomposition of intermediates **i4** and **i5** results in the formation of 1-propynyl boron monoxide ($\text{CH}_3\text{CC}^{11}\text{BO}$; **p3**) and propadienyl boron monoxide ($\text{CH}_2\text{CCH}^{11}\text{BO}$; **p2**) via tight exit transition states in overall exoergic reactions. Note that the energetics of the reactions and the favorable location of the exit transition states of the **i4** \rightarrow **p3** pathway compared to the **i4/i5** \rightarrow **p2** process should favor the formation of the 1-propynyl boron monoxide **p3** ($\text{CH}_3\text{CC}^{11}\text{BO}$) compared to propadienyl boron monoxide ($\text{CH}_2\text{CCH}^{11}\text{BO}$; **p2**) as conformed experimentally depicting fractions of $90 \pm 5\%$ and $10 \pm 5\%$. Finally, please note that neither intermediate **i2** nor **i3** can form isomers **p2** and/or **p3** via atomic hydrogen loss.

To rationalize the methyl group loss and the formation of the ethynyl boron monoxide product (HCC^{11}BO ; **p6**), we can have a closer look at the molecular structures of intermediates **i2** to **i5**. We realize that intermediates **i2** and **i3** hold a methyl group and the boronyl group connected to the C2 carbon atom. The calculations support that intermediate **i3**—either formed from **i2** or **i4**—can undergo unimolecular decomposition via methyl group loss. This process also involves a tight exit transition state; it is 36 kJ mol^{-1} above the energy of the separated products. These data correlated very well with our experimental findings, proposing a tight exit transition state located typically $30\text{--}50 \text{ kJ mol}^{-1}$ above the separated products.

We would like to stress that the experimental findings can all be accounted for by proposing that only intermediates **i1**–**i5** play a role in the reaction mechanism. It is not necessary to involve intermediates **i6**–**i10**, which can be formed via energetically unfavorable hydrogen shifts from **i2** to **i5**, in the reaction mechanism. Is there evidence which supports this conclusion? Considering the RRKM calculations, the associated rate constants for these hydrogen shifts are up to 3 orders of magnitude lower than the competing rate constants for the

unimolecular decomposition. As a typical example, note that the hydrogen migrations from intermediate **i4** to **i6** proceeds via a significant barrier of 178 kJ mol^{-1} ; the rate constant of the competing reaction pathway **i4** \rightarrow **p3**, that is, the decomposition to the products, almost 1000 times larger than the rate constant for the isomerization **i4** \rightarrow **i6** clearly indicates the minor contribution of these hydrogen shifts. Further, the experimental branching ratios of these channels forming $\text{CH}_2\text{CCH}^{11}\text{BO}$ (**p2**), $\text{CH}_3\text{CC}^{11}\text{BO}$ (**p3**), and HCC^{11}BO (**p6**) were derived to be $4 \pm 3\%$, $40 \pm 5\%$, and $56 \pm 15\%$, respectively; these data are in excellent agreement with the calculated branching ratio using statistical RRKM theory yielding 1%, 38%, and 61%, respectively. The branching ratio does not change strongly if intermediates **i6**–**i10** are eliminated from the potential energy surface indicating that the latter do not play any role in the reaction mechanism of boron monoxide with methylacetylene. Finally, it should be noted that the direct hydrogen abstraction channel to forming the propargyl radical (**p4**) cannot be detected by our present experiment due to significant background counts at $m/z = 39$ from dissociative ionization of the methylacetylene parent in the electron impact ionizer.

In conclusion, our study proposes that the reaction is initiated by a barrierless formation of a weakly bound complex **i1**. The boron monoxide radical either adds to the C1 or C2 carbon atom of the carbon–carbon triple bond leading to the formation of two intermediates: **i2** and **i5**, respectively. These structures can isomerize rapidly via low lying transition states involving intermediates **i3** and **i4**. Intermediates **i2**–**i5** undergo unimolecular decomposition through tight exit transition states via atomic hydrogen and methyl loss pathways. The methyl elimination presents the thermodynamically most favorable pathway leading exclusively from intermediate **i3** to ethynyl boron monoxide (HCC^{11}BO) (**p6**). Intermediates **i4** and **i5** can only fragment via atomic hydrogen loss; **i4** can yield both propadienyl boron monoxide ($\text{CH}_2\text{CCH}^{11}\text{BO}$) (**p2**) and 1-propynyl boron monoxide ($\text{CH}_3\text{CC}^{11}\text{BO}$) (**p3**), whereas **i5** is only correlated with the formation of propadienyl boron monoxide ($\text{CH}_2\text{CCH}^{11}\text{BO}$) (**p2**).

The boron monoxide radical presents also an interesting system from the physical organic chemistry viewpoint because of the isoelectronic character of $^{11}\text{BO}(\text{X}^2\Sigma^+)$ and the cyano radical ($\text{CN}; \text{X}^2\Sigma^+$). It is interesting to compare the results from the reactions of $^{11}\text{BO}(\text{X}^2\Sigma^+)$ and $\text{CN}(\text{X}^2\Sigma^+)$ radicals with methylacetylene. The reaction between methylacetylene and the cyano radical was previously investigated by our group.⁸⁶ First, both reactions undergo indirect scattering dynamics via de facto barrierless additions of the radical to the C1 and/or C2 carbon atoms of the carbon–carbon triple bond of the methylacetylene reactant leading to CH_3CCHX and $(\text{CH}_3)\text{-XCCH}$ doublet reaction intermediates ($\text{X} = \text{BO}, \text{CN}$), respectively. These doublet radical intermediates are stabilized by $225\text{--}253 \text{ kJ mol}^{-1}$ ($\text{X} = \text{CN}$) and $170\text{--}197 \text{ kJ mol}^{-1}$ ($\text{X} = \text{BO}$); these energetics indicate the formation of a stronger carbon–carbon ($\text{X} = \text{CN}$) compared to a weaker carbon–boron ($\text{X} = \text{BO}$) single bond; bond strengths differ by typically 50 kJ mol^{-1} . For both systems, the hydrogen elimination channel leads to two distinct isomers: substituted methylacetylenes (CH_3CCX) and substituted allenes (CH_2CCCHX ; $\text{X} = \text{CN}, \text{BO}$) with fractions of about $90 \pm 5\%$ versus $10 \pm 5\%$ (BO reaction) and $80 \pm 10\%$ versus $20 \pm 10\%$ (CN reaction). Also, all decomposition pathways involve tight exit transition states located $15\text{--}31 \text{ kJ mol}^{-1}$ ($\text{X} = \text{BO}$) and $7\text{--}19 \text{ kJ mol}^{-1}$ (X

$= \text{CN}$) above the separated products. Further, the dominant formation of the CH_3CCX isomers is correlated with a hydrogen atom emission almost perpendicularly to the rotational plane of the decomposing intermediate. Finally, both isomers are formed in exoergic reactions ($\text{X} = \text{BO}$: 71 ± 9 and $43 \pm 9 \text{ kJ mol}^{-1}$; $\text{X} = \text{CN}$: 106 ± 10 and $94 \pm 10 \text{ kJ mol}^{-1}$); the enhanced exoergic nature of the cyano radical reaction products is likely the effect of an enhanced carbon–carbon bond strength compared to the weaker carbon–boron single bond formed. Note that both reactions also should yield the thermodynamically most favorable methyl loss pathway forming HCCX ($\text{X} = \text{BO}, \text{CN}$). Whereas the present study clearly exposed the methyl loss pathway, the methyl loss elimination could not be observed in the cyano–methylacetylene reaction. This is a likely effect of the atomic carbon coreactant present in the supersonic cyano radical beam. Here, ground state atomic carbon reacts with methylacetylene leading to C_4H_3 isomers (51 amu) plus atomic hydrogen. On the other hand, the cyano radical reaction and the associated methyl loss channel forms cyanoacetylene (HCCCN) (51 amu). Considering that the atomic carbon beam has a much higher reactant number density in the interaction region of the scattering chamber compared to the cyano radical reactants by a factor of about 20, the signal at $m/z = 51$ is dominated by C_4H_3^+ ions. Future studies of the cyano–methylacetylene system should exploit photolytically generated supersonic cyano radical beams such as from bromo or iodocyanide or cyanogen (NCCN) to probe the methyl loss pathway.

7. SUMMARY

The crossed molecular beam reaction of the boron monoxide radical ($^{11}\text{BO}; \text{X}^2\Sigma^+$) with methylacetylene ($\text{CH}_3\text{CCH}; \text{X}^1\text{A}_1$) was investigated at a collision energy of $22.7 \pm 1.2 \text{ kJ mol}^{-1}$ under single collision conditions. Combined with computational data, the reaction is suggested to proceed without entrance barrier via indirect (complex forming) reaction dynamics by initially forming a $^{11}\text{BOC}_3\text{H}_4$ van-der-Waals collision complex. The latter can isomerize via addition of the boron monoxide radical with its boron atom to the carbon–carbon triple bond of methylacetylene at the C1 and C2 carbon atom. The resulting reaction intermediates can isomerize rapidly via cis–trans isomerization and/or [2,1] and [1,2] shifts of the boronyl group ($-\text{BO}$). The resulting $^{11}\text{BOC}_3\text{H}_4$ doublet radical intermediates underwent unimolecular decomposition involving three competing reaction mechanisms via two distinct atomic hydrogen losses and a methyl group elimination. Utilizing partially deuterated methylacetylene reactants ($\text{CD}_3\text{CCH}; \text{CH}_3\text{CCD}$), we revealed that the addition of $^{11}\text{BO}(\text{X}^2\Sigma^+)$ to the C1 carbon atom of methylacetylene was followed by hydrogen loss from the acetylenic carbon atom (C1) and from the methyl group (C3) leading to 1-propynyl boron monoxide ($\text{CH}_3\text{CC}^{11}\text{BO}$) and propadienyl boron monoxide ($\text{CH}_2\text{CCH}^{11}\text{BO}$), respectively. The addition of $^{11}\text{BO}(\text{X}^2\Sigma^+)$ to the C1 of methylacetylene followed by the migration of the boronyl group to the C2 carbon atom and/or an addition of $^{11}\text{BO}(\text{X}^2\Sigma^+)$ to the sterically less accessible C2 carbon atom of methylacetylene was terminated by a methyl group loss leading to the ethynyl boron monoxide product (HCC^{11}BO) in an overall exoergic reaction ($78 \pm 23 \text{ kJ mol}^{-1}$). The branching ratios of these channels forming $\text{CH}_2\text{CCH}^{11}\text{BO}$, $\text{CH}_3\text{CC}^{11}\text{BO}$, and HCC^{11}BO were derived to be $4 \pm 3\%$, $40 \pm 5\%$, and $56 \pm 15\%$, respectively; these data are in excellent

agreement with the calculated branching ratio using statistical RRKM theory yielding 1%, 38%, and 61%, respectively.

A comparison of the boron monoxide–methylacetylene reaction with the isoelectronic cyano radical–methylacetylene system suggests that, at comparable collision energies, in both reactions the hydrogen atom is eliminated preferentially from the acetylenic carbon atom yielding mainly substituted methylacetylenes (CH_3CCX ; $\text{X} = \text{CN}, \text{BO}$) with fractions of about $90 \pm 5\%$ versus $10 \pm 5\%$ (BO reaction) and $80 \pm 10\%$ versus $20 \pm 10\%$ (CN reaction) compared to the less important hydrogen loss from the methyl group forming substituted allenes (CH_2CCCHX ; $\text{X} = \text{CN}, \text{BO}$). These observations give scope for further investigations to the crossed molecular beam experiments of boron monoxide radical with substituted alkenes and alkynes and a comparison of the reaction dynamics with those of the isoelectronic cyano radical reactant. The detailed exposure of the reaction mechanisms, products, reaction energies, rate constants, and branching ratios of organyl boronyl molecules will provide a key to establish novel combustion models of boron based rocket propulsion systems.

■ ASSOCIATED CONTENT

Supporting Information

Cartesian coordinates in angstroms of reactants, intermediates, products, and transition states optimized at CCSD(T)-fc/cc-pVTZ and relative energies in kJ mol^{-1} with respect to reactants are available. Also the rate constant of each reaction pathway at the collision energy 22.7 kJ mol^{-1} and the computed branching ratios are listed. This material is available free of charge via the Internet at <http://pubs.acs.org>.

■ AUTHOR INFORMATION

Notes

The authors declare no competing financial interest.

■ ACKNOWLEDGMENTS

This work was supported by the Air Force Office of Scientific Research (FA9550-12-1-0213 to University of Hawai'i at Manoa and FA-9550-11-1-0065 to University of Florida).

■ REFERENCES

- (1) Price, E. W. *Fundamentals of Solid-Propellant Combustion (Progress in Astronomy and Aeronautics)*; AIAA: Reston, VA, 1984; Vol. 90, pp 479–513.
- (2) Young, G.; Sullivan, K.; Zacharia, M. R.; Yu, K. Combustion Characteristic of Boron Nanoparticles. *Combust. Flame* **2009**, *156*, 322–333.
- (3) Hinchey, J. J. Kinetics for the Quenching and Relaxation of Boron Oxide. *J. Chem. Phys.* **1993**, *99*, 4403–4410.
- (4) Ulas, A.; Kuo, K. K.; Gotzmer, C. Ignition and Combustion of Boron Particles in Fluorine Containing Environment. *Combust. Flame* **2001**, *127*, 1935–1957.
- (5) Antaki, P.; Williams, F. A. Observations on the Combustion of Boron Slurry Droplets in Air. *Combust. Flame* **1987**, *67*, 1–8.
- (6) King, M. K. Ignition and Combustion of Boron Particles and Clouds. *J. Spacecraft Rockets* **1982**, *19*, 294–306.
- (7) Turns, S. R.; Holl, J. T.; Solomon, A. S. P.; Faeth, G. M. Gasification of Boron Oxide Drops in Combustion Gases. *Combust. Sci. Technol.* **1985**, *43*, 287–300.
- (8) King, M. K. Boron Ignition and Combustion in Air-Augmented Rocket Afterburners. *Combust. Sci. Technol.* **1972**, *5*, 155–164.
- (9) Li, S. C.; Williams, F. A. *Combustion of Boron-Based Solid Propellants and Fuels*; CRC Press: Boca Raton, FL, 1993; p 248.
- (10) Macek, A.; Semple, J. M. Combustion of Boron Particles at Atmospheric Pressure. *Combust. Sci. Technol.* **1969**, *1*, 181–191.
- (11) Macek, A.; Semple, J. M. *Combustion of Boron Carbide Particles*; Atl. Res. Div., Susquehanna Corp.: Alexandria, VA, 1971.
- (12) Macek, A.; Semple, J. M. Combustion of Boron Particle at Elevated Pressures. *Proc. Combust. Inst.* **1971**, *13*, 859–868.
- (13) Macek, A. Combustion of Boron Particles: Experiments and Theory. *Proc. Combust. Inst.* **1972**, *14*, 1401–1411.
- (14) Yeh, C. L.; Kuo, K. K. Ignition and Combustion of Boron Particles. *Prog. Energy Combust. Sci.* **1996**, *22*, 511–541.
- (15) King, M. K. Boron Particle Ignition in Hot Gas Streams. *Combust. Sci. Technol.* **1973**, *8*, 255–273.
- (16) Zhou, W.; Yetter, R. A.; Dryer, F. L.; Rabitz, H.; Brown, R. C.; Kolb, C. E. Multi-Phase Model for Ignition and Combustion of Boron Particles. *Combust. Flame* **1999**, *117*, 227–243.
- (17) Zhou, W.; Yetter, R. A.; Dryer, F. L.; Rabitz, H.; Brown, R. C.; Kolb, C. E. Ignition and Combustion of Boron Particles in Fluorine Containing System. *Chem. Phys. Proc. Combust.* **1996**, 495–498.
- (18) Zhou, W.; Yetter, R. A.; Dryer, F. L.; Rabitz, H.; Brown, R. C.; Kolb, C. E. Effect of Fluorine on the Combustion of “Clean” Surface Boron Particles. *Combust. Flame* **1998**, *112*, 507–521.
- (19) Yetter, R. A.; Dryer, F. L.; Rabitz, H.; Brown, R. C.; Kolb, C. E. Effect of Fluorine on the Gasification Rate of Liquid Boron Oxide Droplets. *Combust. Flame* **1998**, *112*, 387–403.
- (20) Brown, R. C.; Kolb, C. E.; Yetter, R. A.; Dryer, F. L.; Rabitz, H. Kinetic Modeling and Sensitivity Analysis for B/H/O/C/F Combination Systems. *Combust. Flame* **1995**, *101*, 221–238.
- (21) Peretz, A. In *Proceedings of the Eighth International Symposium of Air Breathing Engines*, Cincinnati, OH, 1987; pp 398–403.
- (22) Liu, T.-K.; Shyu, I.-M.; Hsia, Y.-S. Effect of Fluorinated Graphite on Combustion of Boron and Boron-Based Fuel-Rich Propellants. *J. Propul. Power* **1996**, *12*, 26–33.
- (23) Krier, H.; Burton, R. L.; Pirman, S. R.; Spalding, M. J. Shock Initiation of Crystalline Boron in Oxygen and Fluorine Compounds. *J. Propul. Power* **1996**, *12*, 672–679.
- (24) Foelsche, R. O.; Burton, R. L.; Krier, H. Boron Particle Ignition and Combustion at 30–150 atm. *Combust. Flame* **1999**, *117*, 32–58.
- (25) Hussmann, B.; Pfitzner, M. Extended Combustion Model for Single Boron Particles - Part I: Theory. *Combust. Flame* **2010**, *157*, 803–821.
- (26) Hussmann, B.; Pfitzner, M. Extended Combustion Model for Single Boron Particles - Part II: Validation. *Combust. Flame* **2010**, *157*, 822–833.
- (27) Yetter, R.; Rabitz, H.; Dryer, F.; Brown, R.; Kolb, C. E. Kinetics of High-Temperature B/O/H/C Chemistry. *Combust. Flame* **1991**, *83*, 43–62.
- (28) Yetter, R.; Dryer, F.; Rabitz, H. A Comprehensive Reaction Mechanism For Carbon Monoxide/Hydrogen/Oxygen Kinetics. *Combust. Sci. Technol.* **1991**, *79*, 97–128.
- (29) Brown, R. C.; Kolb, C. E.; Cho, S. Y.; Yetter, R. A.; Dryer, F. L.; Rabitz, H. Kinetic Model for Hydrocarbon-Assisted Particulate Boron Combustion. *Int. J. Chem. Kinet.* **1994**, *26*, 319–332.
- (30) Brown, R. C.; Kolb, C. E.; Rabitz, H.; Cho, S. Y.; Yetter, R. A.; Dryer, F. L. Kinetic Model of Liquid B_2O_3 Gasification in a Hydrocarbon Combustion Environment: I. Heterogeneous Surface Reaction. *Int. J. Chem. Kinet.* **1991**, *23*, 957–970.
- (31) Balucani, N.; Asvany, O.; Lee, Y. T.; Kaiser, R. I.; Galland, N.; Hannachi, Y. Observation of Borirene from Crossed Beam Reaction of Boron Atoms with Ethylene. *J. Am. Chem. Soc.* **2000**, *122*, 11234–11235.
- (32) Sillars, D.; Kaiser, R. I.; Galland, N.; Hannachi, Y. Crossed-Beam Reaction of Boron Atoms, $\text{B}(^2\text{P}_1)$, with Dimethylacetylene, CH_3CCCH_3 (X^1A_g): Untangling the Reaction Dynamics to Form the 1,2-Dimethylene-3-bora-cyclopropane Molecule. *J. Phys. Chem. A* **2003**, *107*, 5149–5156.
- (33) Bettinger, H. F.; Kaiser, R. I. Reaction of Benzene and Boron Atom: Mechanism of Formation of Benzoborirene and Hydrogen Atom. *J. Phys. Chem. A* **2004**, *108*, 4576–4586.
- (34) Kaiser, R. I.; Balucani, N.; Galland, N.; Caralp, F.; Rayez, M. T.; Hannachi, Y. Unraveling the Chemical Dynamics of Bimolecular

Reactions of Ground State Boron Atoms, $B(^2P_1)$, with Acetylene, $C_2H_2(X^1\Sigma_g^+)$. *Phys. Chem. Chem. Phys.* **2004**, *6*, 2205–2210.

(35) Zhang, F.; Gu, X.; Kaiser, R. I.; Bettinger, H. A. Reinvestigation of the Gas Phase Reaction of Boron Atoms, $^{11}B(^2P_1)/^{10}B(^2P_1)$ with Acetylene, $C_2H_2(X^1\Sigma_g^+)$. *Chem. Phys. Lett.* **2007**, *450*, 178–185.

(36) Zhang, F.; Guo, Y.; Gu, X.; Kaiser, R. I. A Crossed Molecular Beam Study on the Reaction of Boron Atoms, $B(^2P_1)$, with Benzene, $C_6H_6(X^1A_{1g})$, and D6-Benzene $C_6D_6(X^1A_{1g})$. *Chem. Phys. Lett.* **2007**, *440*, 56–63.

(37) Zhang, F.; Gu, X.; Kaiser, R. I.; Balucani, N.; Huang, C. H.; Kao, C. H.; Chang, A. H. H. A Crossed Molecular Beam Study on the Reaction of Boron Atoms with Methylacetylene and Partially Deuterated Methylacetylene. *J. Phys. Chem. A* **2008**, *112*, 3837–3845.

(38) Balucani, N.; Zhang, F.; Kaiser, R. I. Elementary Reactions of Boron Atoms with Hydrocarbons - Toward the Formation of Organo-Boron Compounds. *Chem. Rev.* **2010**, *110*, 5107–5127.

(39) Bauer, S. H. Oxidation of B, BH, BH_2 , and B_mH_n Species: Thermochemistry and Kinetics. *Chem. Rev.* **1996**, *96*, 1907–1916.

(40) Chin, C.-H.; Mebel, A. M.; Hwang, D.-Y. Theoretical Study of the Reaction Mechanism of BO, B_2O_2 , and BS with H_2 . *J. Phys. Chem. A* **2004**, *108*, 473–483.

(41) Garland, N. L.; Stanton, C. T.; Nelson, H. H.; Page, M. Temperature Dependence of the Kinetics of the Reaction Boron Monoxide + Hydrogen \rightarrow Oxoborane + Atomic Hydrogen. *J. Chem. Phys.* **1991**, *95*, 2511–2515.

(42) Parker, D. S. N.; Zhang, F.; Maksyutenko, P.; Kaiser, R. I.; Chang, A. H. H. A Crossed Beam and Ab Initio Investigation of the Reaction of Boron Monoxide (BO) with Acetylene (C_2H_2). *Phys. Chem. Chem. Phys.* **2011**, *13*, 8560–8570.

(43) Parker, D. S. N.; Zhang, F.; Maksyutenko, P.; Kaiser, R. I.; Chen, S. H.; Chang, A. H. H. A Crossed Beam and Ab Initio Investigation on the Formation of Vinyl Boron Monoxide (C_2H_3BO) via Reaction of Boron Monoxide (BO) with Ethylene (C_2H_4). *Phys. Chem. Chem. Phys.* **2012**, *14*, 11099–11106.

(44) Huang, L. C. L.; Asvany, O.; Chang, A. H. H.; Balucani, N.; Lin, S. H.; Lee, Y. T.; Kaiser, R. I.; Osamura, Y. Crossed Beam Reaction of Cyano Radicals with Hydrocarbon Molecules. IV. Chemical Dynamics of Cyanoacetylene ($HCCCN$; $X^1\Sigma^+$) Formation from Reaction of $CN(X^2\Sigma^+)$ with Acetylene, $C_2H_2(X^1\Sigma_g^+)$. *J. Chem. Phys.* **2000**, *113*, 8656–8666.

(45) Gu, X.; Guo, Y.; Zhang, F.; Mebel, A. M.; Kaiser, R. I. Reaction Dynamics of Carbon-Bearing Radicals in Circumstellar Envelopes of Carbon Stars. *Faraday Discuss.* **2006**, *133*, 245–275.

(46) Gu, X.; Guo, Y.; Kaiser, R. I. Mass Spectrum of the Butadiynyl Radical (C_4H ; $X^2\Sigma^+$). *Int. J. Mass Spectrom.* **2005**, *246*, 29–34.

(47) Gu, X. B.; Guo, Y.; Kawamura, E.; Kaiser, R. I. Design of a Convection-Cooled, Cluster-Based Voltage Divider Chain for Photomultiplier Tubes. *Rev. Sci. Instrum.* **2005**, *76*, 083115/1–6.

(48) Guo, Y.; Gu, X.; Kaiser, R. I. Mass Spectrum of the 1-Butene-3-yne-2-yl Radical ($i-C_4H_3$; X^2A'). *Int. J. Mass Spectrom.* **2006**, *249/250*, 420–425.

(49) Guo, Y.; Gu, X.; Kawamura, E.; Kaiser, R. I. Design of a Modular and Versatile Interlock System for Ultrahigh Vacuum Machines: A Crossed Molecular Beam Setup as a Case Study. *Rev. Sci. Instrum.* **2006**, *77*, 034701/1–9.

(50) Gu, X.; Guo, Y.; Kawamura, E.; Kaiser, R. I. Characteristics and Diagnostics of an Ultrahigh Vacuum Compatible Laser Ablation Source for Crossed Molecular Beam Experiments. *J. Vac. Sci. Technol.* **2006**, *24*, 505–511.

(51) Proch, D.; Trickl, T. A High-Intensity Multi-Purpose Piezoelectric Pulsed Molecular Beam Source. *Rev. Sci. Instrum.* **1989**, *60*, 713–716.

(52) Maksyutenko, P.; Parker, D. S. N.; Zhang, F.; Kaiser, R. I. An LIF Characterization of Supersonic BO and CN Radical Sources for Crossed Beam Studies. *Rev. Sci. Instrum.* **2011**, *82*, 083107/1–7.

(53) Tan, X. *CyberWit*, 1.4.1.1 ed.; CyberWit, Inc.: Acton, MA, 2004.

(54) Vernon, M. Thesis, University of California, Berkeley, CA, 1981.

(55) Weis, M. S. Ph.D. Thesis, University of California, Berkeley, CA, 1986.

(56) Krajnovich, D.; Huisken, F.; Zhang, Z.; Shen, Y. R.; Lee, Y. T. Competition Between Atomic and Molecular Chlorine Elimination in the Infrared Multiphoton Dissociation of CF_2Cl_2 . *J. Chem. Phys.* **1982**, *77*, 5977–5989.

(57) Raghavachari, K.; Trucks, G. W.; Pople, J. A.; Head-Gordon, M. A Fifth-Order Perturbation Comparison of Electron Correlation Theories. *Chem. Phys. Lett.* **1989**, *157*, 479–483.

(58) Bartlett, R. J.; Watts, J. D.; Kucharsky, S. A.; Noga, J. Non-Iterative Fifth-Order Triple and Quadruple Excitation Energy Corrections in Correlated Methods. *Chem. Phys. Lett.* **1990**, *165*, 513–522.

(59) Gauss, J.; Lauderdale, W. J.; Stanton, J. F.; Watts, J. D.; Bartlett, R. J. Analytic Energy Gradients for Open-shell Coupled-Cluster Singles and Doubles (CCSD) Calculations Using Restricted Open-Shell Hartree-Fock (ROHF) Reference Functions. *Chem. Phys. Lett.* **1991**, *182*, 207–215.

(60) Watts, J. D.; Gauss, J.; Bartlett, R. J. Coupled-Cluster Methods with Noniterative Triple Excitations for Restricted Open-Shell Hartree-Fock and Other General Single Determinant Reference Functions. Energies and Analytical Gradients. *J. Chem. Phys.* **1993**, *98*, 8718–8733.

(61) Dunning, T. H. Gaussian Basis Sets for Use in Correlated Molecular Calculations. I. The Atoms Boron through Neon and Hydrogen. *J. Chem. Phys.* **1989**, *90*, 1007–1023.

(62) Woon, D. E.; Dunning, T. H., Jr. Gaussian Basis Sets for Use in Correlated Molecular Calculations. V. Core-Valence Basis Sets for Boron through Neon. *J. Chem. Phys.* **1995**, *103*, 4572–4585.

(63) Schwenke, D. W. The Extrapolation of One-Electron Basis Sets in Electronic Structure Calculations: How It Should Work and How It Can Be Made to Work. *J. Chem. Phys.* **2005**, *122*, 014107/1–7.

(64) Bakowies, D. Accurate Extrapolation of Electron Correlation Energies from Small Basis Sets. *J. Chem. Phys.* **2007**, *127*, 164109/1–12.

(65) Noga, J.; Bartlett, R. J. The Full CCSDT Model for Molecular Electronic Structure. *J. Chem. Phys.* **1987**, *86*, 7041–7050.

(66) Watts, J. D.; Bartlett, R. J. The Coupled-Cluster Single, Double, and Triple Excitation Model for Open-Shell Single Reference Functions. *J. Chem. Phys.* **1990**, *93*, 6104–6105.

(67) Scuseria, G. E.; Schaefer, H. F., III. A New Implementation of the Full CCSDT Model for Molecular Electronic Structure. *Chem. Phys. Lett.* **1988**, *152*, 382–386.

(68) Merrick, J. P.; Moran, D.; Radom, L. An Evaluation of Harmonic Vibrational Frequency Scale Factors. *J. Phys. Chem. A* **2007**, *111*, 11683–11700.

(69) Ruscic, B.; Pinzon, R. E.; Laszewski, G. V.; Kodeboyina, D.; Burcat, A.; Leahy, D.; Montoya, D.; Wagner, A. F. Active Thermochemical Tables: Thermochemistry for the 21st Century. *J. Phys.: Conf. Series* **2005**, *16*, 561–570.

(70) Ruscic, B.; Pinzon, R. E.; Morton, M. L.; Laszewski, G. V.; Bittner, S. J.; Nijssure, S. G.; Amin, K. A.; Minkoff, M.; Wagner, A. F. Introduction to Active Thermochemical Tables: Several “Key” Enthalpies of Formation Revisited. *J. Phys. Chem. A* **2004**, *108*, 9979–9997.

(71) Ruscic, B.; Pinzon, R. E.; Morton, M. L.; Srinivasan, N. K.; Su, M.-C.; Sutherland, J. W.; Michael, J. V. Active Thermochemical Tables: Accurate Enthalpy of Formation of Hydroperoxyl Radical, HO_2 . *J. Phys. Chem. A* **2006**, *110*, 6592–6601.

(72) Harding, M. E.; Vásquez, J.; Ruscic, B.; Wilson, A. K.; Gauss, J.; Stanton, J. F. High-Accuracy Extrapolated Ab Initio Thermochemistry. III. Additional Improvements and Overview. *J. Chem. Phys.* **2008**, *128*, 114111/1–15.

(73) ACES II is a program product of the Quantum Theory Project, University of Florida. Stanton, J. F.; Gauss, J.; Perera, S. A.; Watts, J. D.; Yau, A. D.; Nooijen, M.; Oliphant, N.; Szalay, P. G.; Lauderdale, W. J.; Gwaltney, S. R. et al.; Integral packages included are VMOL (Almlöf, J.; Taylor, P. R.); VPROPS (Taylor, P.); ABACUS (Helgaker, T.; Jensen, H. J. Aa.; Jørgensen, P.; Olsen, J.; Taylor, P. R.); HONDO/GAMESS (Schmidt, M. W.; Baldrige, K. K.; Boatz, J. A.; Elbert, S. T.;

Gordon, M. S.; Jensen, J. J.; Koseki, S.; Matsunaga, N.; Nguyen, K. A.; Su, S., et al.).

(74) Valiev, M.; Bylaska, E. J.; Govind, N.; Kowalski, K.; Straatsma, T. P.; van Dam, H. J. J.; Wang, D.; Nieplocha, J.; Apra, E.; Windus, T. L.; et al. NWChem: A Comprehensive and Scalable Open-Source Solution for Large Scale Molecular Simulations. *Comput. Phys. Commun.* **2010**, *181*, 1477–1489.

(75) Hirata, S. Tensor Contraction Engine: Abstraction and Automated Parallel Implementation of Configuration-Interaction, Coupled-Cluster, and Many-Body Perturbation Theories. *J. Phys. Chem. A* **2003**, *107*, 9887–9897.

(76) CFOUR, a quantum chemical program package written by Stanton, J. F.; Gauss, J.; Harding, M. E.; Szalay, P. G. with contributions from Auer, A. A.; Bartlett, R. J.; Benedikt, U.; Berger, C.; Bernholdt, D. E.; Bomble, Y. J.; Christiansen, O.; Heckert, M.; Heun, O.; Huber, C. et al. and the integral packages MOLECULE (Almlöf, J.; Taylor, P. R.), PROPS (Taylor, P. R.), ABACUS (Helgaker, T.; Jensen, H. J. A.; Jørgensen, P.; Olsen, J.), and ECP routines by Mitin, A. V.; van Wüllen, C. For the current version, see <http://www.cfour.de>.

(77) Levine, R. D. *Molecular Reaction Dynamics*; Cambridge University Press: Cambridge, U.K., 2005.

(78) Nguyen, T. L.; Mebel, A. M.; Lin, S. H.; Kaiser, R. I. Product Branching Ratios of the $C(^3P) + C_2H_3(^2A')$ and $CH(^2\Pi) + C_2H_2(^1\Sigma_g^+)$ Reactions and Photodissociation of $H_2CC=CH(^2B_1)$ at 193 and 242 nm: An Ab Initio/RRKM Study. *J. Phys. Chem. A* **2001**, *105*, 11549–11559.

(79) Eyring, H.; Lin, S. H.; Lin, S. M. *Basic Chemical Kinetics*; Wiley: New York, 1980.

(80) Eckart, C. The Theory and Calculation of Screening Constants. *Phys. Rev.* **1930**, *36*, 878–892.

(81) Wang, P. S. C. Ground-State Energy of Three Atomic Helium Molecules. *J. Chem. Phys.* **1970**, *53*, 466–467.

(82) Kislov, V. V.; Mebel, A. M. The programs RRKM_01 and BRANCH were supplied by the Mebel group at Florida International University, Miami, FL.

(83) Chang, A. H. H.; Mebel, A. M.; Yang, X. M.; Lin, S. H.; Lee, Y. T. Ab Initio/RRKM Approach toward the Understanding of Ethylene Photodissociation. *J. Chem. Phys.* **1998**, *109*, 2748–2761.

(84) Kaiser, R. I.; Mebel, A. M. The Reactivity of Ground-State Carbon Atoms with Unsaturated Hydrocarbons in Combustion Flames and in the Interstellar Medium. *Int. Rev. Phys. Chem.* **2002**, *21*, 307–356.

(85) Miller, W. B.; Safron, S. A.; Herschbach, D. R. Exchange Reactions of Alkali Atoms with Alkali Halides. Collision Complex Mechanism. *Discuss. Faraday Soc.* **1967**, *44*, 108–122.

(86) Balucani, N.; Asvany, O.; Kaiser, R. I.; Osamura, Y. Formation of Three C_4H_3N Isomers from the Reaction of $CN(X^2\Sigma^+)$ with Allene, H_2CCCH_2 (X^1A_1), and Methylacetylene, CH_3CCH (X^1A_1): A Combined Crossed Beam and Ab Initio Study. *J. Phys. Chem. A* **2002**, *106*, 4301–4311.